# Probabilistic modeling of surface effects in nano-reinforced materials

Tien-Thinh Le

# Probabilistic modeling of surface effects in nano-reinforced materials

Tien-Thinh Le[a,*]

[a] *Université Paris-Est, Laboratoire Modélisation et Simulation Multi Echelle, MSME UMR 8208 CNRS, 5 bd Descartes, 77454 Marne-la-Vallée, France*

## Abstract

This work is concerned with multiscale analysis of nano-reinforced heterogeneous materials. Such materials exhibit surface effects that are typically taken into account through interface models in mean-field homogenization theories. However, both experiments and numerical simulations demonstrate the existence of a perturbed area at the boundary between the inclusion and the matrix phase. This area is modeled as an interphase whose elastic properties randomly fluctuate from point to point and must be characterized from a probabilistic standpoint. In this study, we therefore address (i) the stochastic modeling of the interphase and (ii) the study of the relationship between the random interphase model and a deterministic interface model. The aim of this work is twofold. First of all, we are interested in constructing a probabilistic model for the matrix-valued random field, modeling the elastic properties of the interphase. Then, this model is used to perform a parametric study for the apparent tensor associated with the microstructure. Simulations are specifically used to characterize the influence of both the random interphase and interface models on the material's overall properties. When the interface model is consistent from a physical point of view, the associated elastic surface properties are computed by solving an optimization problem involving the effective properties of the random medium.

*Keywords:* Nano-reinforced materials, Mechanical properties, Probabilistic model, Interphase - Interface, Random field

*Corresponding author
*Email address:* tien-thinh.le@univ-paris-est.fr (Tien-Thinh Le)

## 1. Introduction

Nanocomposites are heterogeneous materials, generally of the matrix-inclusions type, in which the reinforcements are of nanometric size – with a characteristic size typically less than 100 $nm$ [1]. Unlike conventional composite materials reinforced by micro- and millimetric inclusions, these materials exhibit novel multi-physical phenomena that are linked to interactions at the smallest scales [1]. These interactions cause significant alterations of the local physical properties – in particular, of the matrix phase (for instance, transition and/or modification of phase, specific conformation, modification of the degree of crystallinity for an organic polymer matrix, etc.) [2, 3, 4]. Generally, these alterations give rise to significant improvement of certain macroscopic properties (mechanical, optical, electrical, etc.). From a mechanical point of view, numerous experimental and numerical studies have shown that this marked improvement in properties is exhibited more prominently when the inclusions are small in size (for a sufficiently large volume fraction of reinforcements): this is called the nano-effect [5, 6, 7, 8, 9]. The characterization and modeling of the nano-effect, and its use in optimizing certain key properties, has given rise to a very large number of works spanning the boundaries between scientific communities (chemists, physico-chemists, mechanics, etc.), as well as growing industrial interest [5].

One of the most widely documented aspects in the literature, both from an experimental and a numerical point of view, is the existence of an interphase surrounding the heterogeneities. From experimental investigations, the interphase has been characterized as a disturbed area of the matrix phase near the surface of the inclusions, highlighted by the measurements of the local mobility of atoms, using Nuclear Magnetic Resonance, for instance, [4, 10, 2, 3]. Berriot et al. [10] demonstrated a notable decrease in the mobility of the polymer chains in the vicinity of the nanofillers, together with a modification of the local density. The thickness of this interphase zone remained constant (to within the capabilities of the measuring equipment) when the size of the reinforcements was modified. Consequently, a reduction in size of the reinforcements in-

duces an increase of their specific surface. This effect, called surface effect, is commonly invoked in the development of multiscale models to explain the aforementioned nano-effect [11]. These experimental observations on the interphase in the nanocomposite have also been thoroughly correlated by numerical simulation. Various investigations in Molecular Dynamics such as [12, 13, 14, 15] have also highlighted a modified zone of the polymer matrix surrounding the nanofillers. More precisely, they have found a preferential orientation of the polymer chain segments, situated on the plane tangential to the vector normal to the surface of the nanoparticles.

For such nano-reinforced materials, interactions at small scales (between nanofillers and the matrix, or between different nanofillers) are no longer negligible and must be interpreted and modeled in a multi-scale framework [16, 17, 18, 19, 20]. From the standpoint of continuum mechanics, two types of approaches have been developed in order to: (i) estimate the effective properties of nano-reinforced materials and (ii) take account of the surface effect, mentioned above. One category of approach is based on the integration of interface models in classical micro-mechanical formulations (e.g. of similar type to Eshelby's inclusion). The formulation is generally based on the introduction of a Gurtin-Murdoch surface elasticity [21, 22] to obtain an explicit dependence of the characteristic dimensions of the nanometric inclusions on the effective properties [23, 24, 25]. Many investigations of this class can be found in the literature; see e.g. [26, 27, 28, 29, 30]. In a second category of approach, the interphase is considered as an additional finite-volume phase, exhibiting a positive-definite elasticity tensor [20, 14, 31, 32]. In this case, the equivalent properties can be determined by micromechanical frameworks, such as the generalized self-consistent scheme [33, 34, 35, 36, 37, 38] or a numerical finite element scheme [14, 39, 32, 40, 41, 31, 42].

In this work, we are interested in the multi-scale modeling of heterogeneous materials with nanoscopic particle reinforcements. As revealed in the literature, such materials exhibit surface effects that have widely been demonstrated through experimentation (see, for instance, [10]). In the case of polymer matrices, recent contributions have shown that the strengthening effect is notably due to a local modification of the distri-

bution of the polymer chains surrounding the nanofillers. Indeed, Ciprari et al. [43] found a modification of molecular chain entanglements around alumina and magnetite nanoinclusions embedded in poly(methyl methacrylate) and polystyrene matrices (also see Riggleman et al. [44] for molecular chain entanglements around nanoparticles). Moreover, local disarrangement in the mobility of the polymer chains, as well as density fluctuations vanishing outside the vicinity of the inclusions in nanocomposites, have been observed in [12, 45, 35, 46, 47] through numerical simulation. From the modeling point of view, most models developed for the modified matrix area are deterministic [32, 48, 49, 5] despite the stochastic nature of the interaction between the matrix and the nanoparticle [50, 51]. Thus, in this study, we propose a probabilistic model of the interphase whose mechanical properties exhibit random spatial fluctuations [52, 53, 54]. Moreover, the hypothesis of separation of scale in the random interphase, which has not been sufficiently well documented in the literature, can be investigated with the proposed stochastic model and spatial correlation structures. On the other hand, one may legitimately question the relationship between such a stochastic interphase model and the interface models [8, 55, 56, 27] typically used in homogenization methods in micromechanics. It is worth noting that the mechanical properties of an interface model and those of a finite-volume interphase are usually linked by the interphase thickness [57, 26, 58], though from a deterministic point of view. In addition, such a connection depends on several factors, such as the level of anisotropy and the selection of imperfection types (displacement and/or traction jumps) [16]. Moreover, the question remains open as to the spatial correlation structures in the context of which the equivalent interface model can be derived from the random interphase. Hence, in this study, we employ an optimization procedure to identify, if possible, the mechanical properties of an equivalent coherent interface model from the stochastic interphase. This work constitutes a contribution to this problem, restricted here to the case of 2D linear elasticity.

This paper is organized as follows. Section 2 is devoted to the modeling of mechanical properties of the interphase using a probabilistic model. The stochastic homogenization of nano-reinforced materials is also introduced in this section. Finally, the

results of the parametric study on the apparent properties of heterogeneous materials is presented in Section 3, together with an identification of an equivalent interface model.

## 2. Materials and methods

### *2.1. Microstructure of heterogeneous material*

In this work, we consider a heterogeneous material made up of three phases: a matrix, a spherical inclusion and an interphase (see Fig. 1). It is worth noting that the interphase thickness remains an open question, in the sense that it depends on the selected criterion. Voyiatzis et al. [59] proved that the thickness of the interphase depends on the properties being monitored. The interphase thickness can be determined by characterizing fluctuations in mass density [12], preferred segmental orientation [45] , molecular chain entanglements [43] or the decrease in mean-square displacements [60] . Each of these criteria may yield a different estimate of the interphase thickness, and the quantitative definition of this property can impact the modeling methodology. In order to simplify the analysis, and based on the results presented in [12, 32], it is further assumed that the interphase is of constant thickness.

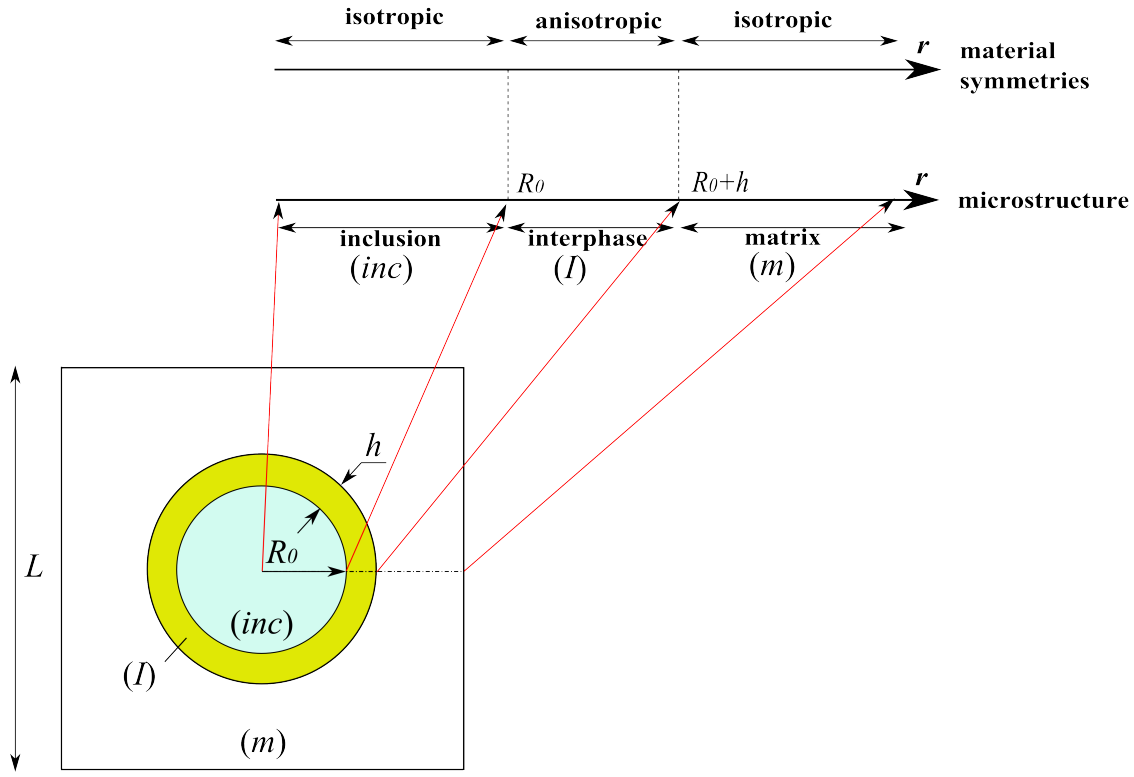


**Fig. 1:** Microstructure of nano-reinforced material considered in this study.

The geometric parameters describing the microstructure are then the radius of the nanoscopic reinforcement $R_0$, the surface fraction $f_i$ of the inclusion, the thickness $h$ of the interphase and finally the size of the domain $L$. We also use the notation $(I)$ to denote the geometric domain occupied by the interphase, identified in a cylindrical coordinate system:

$$(I) := \{(r\cos\theta, r\sin\theta) \mid r \in [R_0; R_0 + h],\ \theta \in [0; 2\pi]\} \tag{1}$$

In this work, the matrix and inclusion phases are considered isotropic. On the other hand, spatial and random fluctuations are presented in the interphase. Consequently, the interphase exhibits anisotropic properties, as shown in Fig. 1.

*2.2. Probabilistic modeling for mechanical properties of interphase*

In this section, we construct a probabilistic model for the mechanical properties of the interphase. In general, there is no separation of scale for the equivalent properties of the interphase, these properties then being qualified as "apparent" [61, 62, 63, 64]. This non-separation of scale means that the "equivalent" material for the interphase must be modeled as a random field, whose levels of anisotropy and statistical fluctuations are likely to evolve with the spatial coordinates [65, 66]. We are therefore interested in the modeling of a random field $\left\{[\mathbf{C}^{\text{int}}(\mathbf{x})],\ \mathbf{x} \in (I)\right\}$, with values in space $\mathbb{M}_3^+(\mathbb{R})$ of real $(3 \times 3)$ matrices, symmetrical positive-definite, representing the elastic properties of the interphase. For given $r$ and $\theta$, $[\mathbf{C}^{\text{int}}(r,\theta)]$ is a random matrix, defined by a probability density, which is denoted by $p_{[\mathbf{C}^{\text{int}}]}$. In this work, we follow the construction methodology introduced in Soize 2006 [67], which basically consists of:

- prescribing the family of first-order marginal probability distributions, each element of which is constructed using the principle of Maximum Entropy ([68], [69]).

- introducing statistical dependencies (and correlations) using normalized homogeneous Gaussian fields, called stochastic germs, such that the matrix $[\mathbf{C}^{\text{int}}(\mathbf{x})]$ is expressed algebraically using a measurable non-linear transformation of these germs at the point in question.

We use $\mathcal{S}$ to denote the Shannon's entropy of the probability density function $p$ [69]:

$$\mathcal{S}(p) = -\int_{\mathbb{M}_3^+(\mathbb{R})} p([C]) \ln(p([C]))\mathrm{d}[C], \tag{2}$$

where $\mathrm{d}[C]$ is the volume element in $\mathbb{M}_3^+(\mathbb{R})$. In order to proceed with the construction of the model, it is assumed that $[\mathbf{C}^{\text{int}}]$ satisfies $\lambda$ algebraic constraints, expressed in the form of mathematical expectations and defining the objectively available information in $[\mathbf{C}^{\text{int}}]$. The probability density function $p_{[\mathbf{C}^{\text{int}}]}$ is then obtained as the solution to the optimization problem (using the principle of Maximum Entropy):

$$p_{[\mathbf{C}^{\text{int}}]} = \arg\max_{p \in \mathcal{C}_{ad}} \mathcal{S}(p), \tag{3}$$

where $\mathcal{C}_{ad}$ is the admissible space of all the functions of $\mathbb{M}_3^+(\mathbb{R})$ in $\mathbb{R}^+$ such that all the constraints are satisfied. More specifically, we consider the following constraints [70, 71]:

$$\int_{\mathbb{M}_3^+(\mathbb{R})} p_{[\mathbf{C}^{\text{int}}]}([C])\mathrm{d}[C] = 1,$$

$$\mathbb{E}\{[\mathbf{C}^{\text{int}}(\mathbf{x})]\} = [\underline{C}(\mathbf{x})] \in \mathbb{M}_3^+(\mathbb{R}),$$

$$\mathbb{E}\{\log(\det([\mathbf{C}^{\text{int}}(\mathbf{x})]))\} = \nu, \ |\nu| < +\infty,$$

where $\mathbb{E}$ denotes the mathematical expectation operator. We then obtain the following probability density function [65, 72]:

$$p_{[\mathbf{C}^{\text{int}}]}([C]) = \mathbb{1}_{\mathbb{M}_3^+(\mathbb{R})}([C]) \times c \times (\det[C])^{B/\delta^2-2} \times \exp\left(-\frac{B}{\delta^2} \ll [\underline{C}]^{-1}, [C] \gg\right), \tag{4}$$

in which $\mathbb{1}_{\mathbb{M}_3^+(\mathbb{R})}([C])$ is equal to 1 if $[C] \in \mathbb{M}_3^+(\mathbb{R})$ and is equal to zero if $[C] \notin \mathbb{M}_3^+(\mathbb{R})$, $c$ is the normalization constant, $\delta$ is the parameter controlling the level of statistical fluctuations, the parameter $B = \frac{1}{2} + \frac{(\mathrm{tr}[\underline{C}])^2}{2\mathrm{tr}([\underline{C}]^2)}$ and $\ll \cdot, \cdot \gg$ denotes the dot product in $\mathbb{M}_3^+(\mathbb{R})$. Furthermore, following the construction methodology in Soize [67], a non-linear transformation $\mathbf{T}$ can be introduced such that:

$$[\mathbf{C}^{\text{int}}(\mathbf{x})] = \mathbf{T}\left(\xi_1(\mathbf{x}), \ldots, \xi_6(\mathbf{x})\right) \tag{5}$$

for every $\mathbf{x}$ in the interphase area $(I)$, where $\{\xi_1(\mathbf{x}), \mathbf{x} \in \mathbb{R}^2\}, \ldots, \{\xi_6(\mathbf{x}), \mathbf{x} \in \mathbb{R}^2\}$ are homogeneous and normalized real scalar Gaussian fields, called stochastic germs. The model therefore depends on the average function $\mathbf{x} \mapsto [\underline{C}(\mathbf{x})]$ of the parameter $\delta$ and correlation functions of the stochastic germs. We write $(r, \theta; r', \theta') \mapsto \rho^{\xi_i}(r, \theta; r', \theta')$ to denote the normalized correlation function of the germ $\{\xi_i(\mathbf{x}), \mathbf{x} \in \mathbb{R}^2\}$. Here, we adopt a hypothesis of separation of the variables [67, 73] – that is:

$$\rho^{\xi_i}(r,\theta;r',\theta') := \rho_r^{\xi_i}(r,r') \times \rho_\theta^{\xi_i}(\theta,\theta'). \tag{6}$$

Based on the results presented in Brown et al. [12], the hypothesis of orthoradial stationarity can be employed. Therefore, we denote $\rho_\theta^{\xi_i}(\theta,\theta') = \rho_\theta^{\xi_i}(\tau_\theta)$, where $\tau_\theta = |\theta - \theta'|$. Assuming homogeneity in the radial direction, we can denote the same $\rho_r^{\xi_i}(r,r') = \rho_\theta^{\xi_i}(\tau_r)$, with $\tau_r = |r - r'|$. In this work, we use the following algebraic forms [67, 74]:

$$\rho_\theta^{\xi_i}(\tau_\theta) = \cos(2\tau_\theta)\frac{\cosh(\frac{\tau_\theta - \pi}{L_\theta})}{\cosh(\frac{\pi}{L_\theta})}, \text{ and } \rho_r^{\xi_i}(\tau_r) = \frac{4L_r^2}{\pi^2\tau_r^2}\sin^2\left(\frac{\pi\tau_r}{L_r}\right), \tag{7}$$

where $L_r$ and $L_\theta$ are the correlation lengths in the radial and angular directions, respectively, assumed to be identical – for simplicity's sake – for the six stochastic germs mentioned above.

For illustration purposes, Fig. 2a and Fig. 2b show the correlation functions $\rho_r^{\xi_i}(\tau_r)$ and $\rho_\theta^{\xi_i}(\tau_\theta)$ for different radial and angular correlation lengths, respectively. These illustrations offer a clear visualization of the incidence of each parameter on the correlation structure of the considered Gaussian random field.

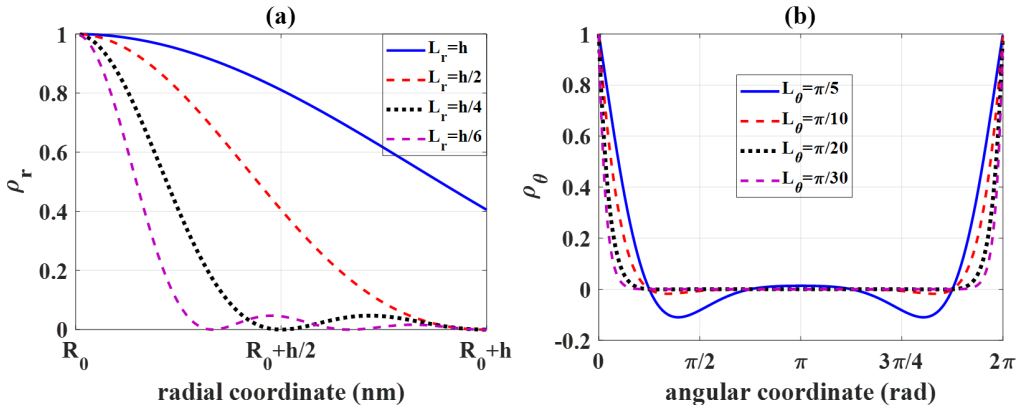


**Fig. 2:** Correlation function for different correlation lengths: (a) in radial and (b) angular directions, respectively.

### *2.3. Stochastic homogenization scheme*

In this section, we briefly summarize the homogenization procedure for estimating the macroscopic properties of heterogeneous materials in continuum mechanics. The

inner domain and its boundary are denoted $\Omega$ and $\partial\Omega$ (also see Fig. 1). It is noteworthy that the domain $\Omega$ presents significant statistical fluctuations in the interphase zone. Consequently, the macroscopic properties of the heterogeneous material are qualified as *apparent* [75, 76, 77]. The stochastic boundary value problem [75, 78, 79, 80] is then written:

$$-\text{div}\,[\boldsymbol{\sigma}(\boldsymbol{x})] = 0 \quad , \quad \forall \boldsymbol{x} \in \Omega \ , \tag{8}$$

$$\boldsymbol{u} = [E]\,.\boldsymbol{x} \quad , \quad \forall \boldsymbol{x} \in \partial\Omega \ , \tag{9}$$

where $\boldsymbol{x} \mapsto [\boldsymbol{\sigma}(\boldsymbol{x})]$ is the local stress field, $\boldsymbol{n}(\boldsymbol{x})$ is the unit vector normal to $\partial\Omega$ at point $\boldsymbol{x}$ and $[E]$ is the macroscopic strain tensor. Hooke's law is then written [81, 82]:

$$[\boldsymbol{\sigma}(\boldsymbol{x})] = [\![\boldsymbol{C}(\boldsymbol{x})]\!] : [\boldsymbol{\varepsilon}(\boldsymbol{x})] \ , \quad \forall \boldsymbol{x} \in \Omega \ , \tag{10}$$

where $[\![\boldsymbol{C}(\boldsymbol{x})]\!]$ is the fourth-order tensor representation of elasticity matrix $[\boldsymbol{C}(\boldsymbol{x})]$. Note that $[\![\boldsymbol{C}(\boldsymbol{x})]\!]$ is random in the interphase zone (i.e. $\boldsymbol{x} \in (I)$), and deterministic in the inclusion and matrix phases, respectively.

It can be shown that a fourth-order localization tensor exists, $\boldsymbol{x} \mapsto [\![\boldsymbol{A}(\boldsymbol{x})]\!]$, relating the microscopic and macroscopic strains such that [83]

$$[\boldsymbol{\varepsilon}(\boldsymbol{x})] = [\![\boldsymbol{A}(\boldsymbol{x})]\!] : [E] \ , \quad \forall \boldsymbol{x} \in \Omega \tag{11}$$

and

$$\frac{1}{|\Omega|} \int_\Omega [\![\boldsymbol{A}(\boldsymbol{x})]\!] \, \mathrm{d}\boldsymbol{x} = [\![I]\!] \ , \tag{12}$$

with $[\![I]\!]$ being the identity tensor. By construction, one has

$$A_{ijk\ell}(\boldsymbol{x}) = \varepsilon_{ij}^{k\ell}(\boldsymbol{x}) \ , \tag{13}$$

where $\boldsymbol{x} \mapsto [\boldsymbol{\varepsilon}^{k\ell}(\boldsymbol{x})]$ is the local strain field solving the mechanical problem defined by Eqs (8 and 10). The macroscopic strain tensor $E^{k\ell}$ is given by:

$$E^{k\ell}{}_{ij} = \frac{1}{2}(\delta_{ik}\delta_{j\ell} + \delta_{i\ell}\delta_{jk}) \ . \tag{14}$$

In this case of 2D linear elasticity, the use of three different values for the macroscopic strain tensor $E^{k\ell}$, with $k$ and $\ell$ in $\{1, 2\}$, can solve the boundary value problem defined by Eqs (8 and 10). The apparent stiffness tensor $[\![\boldsymbol{C}^{\text{app}}]\!]$ is then computed with respect to static uniform boundary conditions [26]:

$$[\![\boldsymbol{C}^{\text{app}}]\!] = \frac{1}{|\Omega|}\int_{\Omega} [\![\boldsymbol{C}(\boldsymbol{x})]\!] : [\![\boldsymbol{A}(\boldsymbol{x})]\!] \, \mathrm{d}\boldsymbol{x} \ . \tag{15}$$

In this work, macroscopic strains were prescribed as follows:

$$E^{11} = \begin{bmatrix} 1 & 0 \\ 0 & 0 \end{bmatrix} ; \ E^{22} = \begin{bmatrix} 0 & 0 \\ 0 & 1 \end{bmatrix} ; \ E^{12} = \begin{bmatrix} 0 & 1/2 \\ 1/2 & 0 \end{bmatrix} \ . \tag{16}$$

Finally, the Monte Carlo method was used to propagate fluctuations in the interphase onto the macroscopic properties of the heterogeneous material. A diagram illustrating the use of the Monte Carlo method is shown in Fig. 3, whereas the statistical convergence analysis of the mean of a random variable W is estimated on the basis of Eq. 17 [84, 85, 86, 87, 88, 89]:

$$n \mapsto ConvMean(n) = \frac{1}{n}\sum_{i=1}^{n} W_i \ , \tag{17}$$

where $n$ is the number of Monte Carlo runs, and $W_i$ is the value of the $i^{th}$ observation of random variable $W$.

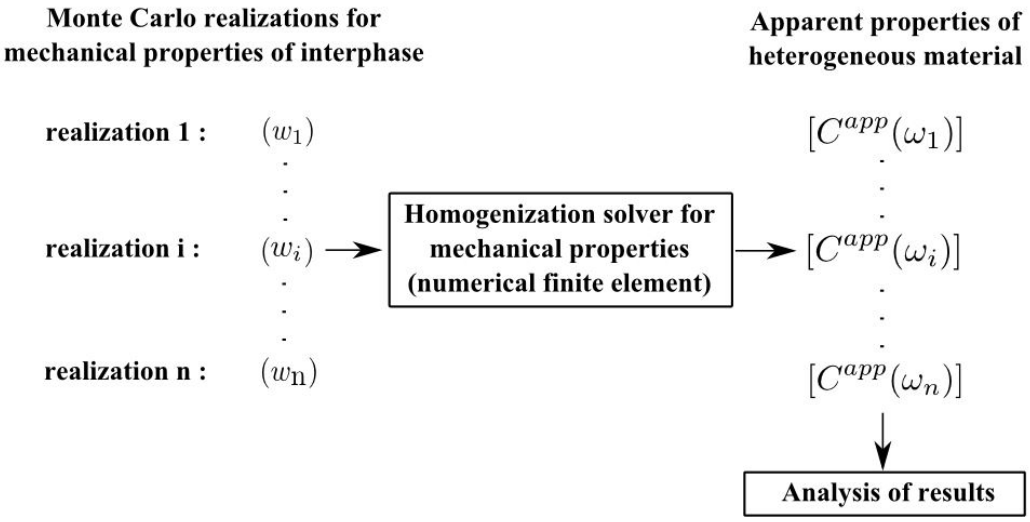


**Fig. 3:** Diagram of using Monte Carlo technique for propagating fluctuations in the interphase to the apparent properties of material.

## 3. Stochastic homogenization and equivalent interface model

### *3.1. Details of numerical study and parametric analysis*

Using the geometric and stochastic models mentioned above, it is now possible to carry out simulations for the microstructure considered. Specifically, we denote $R_0 = 1$ $nm$, $h = 0.5$ $nm$ and $f_i = 0.15$ (see Section 2.1 for details of geometric description). From experimental investigations of interphase thickness, several papers can be referred to, such as Yu et al. [90] for epoxy matrix reinforced with aluminum oxide nanoparticles, exhibiting an interphase of 0.67 $nm$, or Tsai and Tzeng [91] for polyimide reinforced by silica nanoparticles, exhibiting an interphase of 3.2-4.1 $nm$).

Additionally, multiple combinations of correlation lengths are used as a parametric analysis for the random properties in the interphase: $L_r \in \{h, h/2, h/4, h/6\}$, $L_\theta \in \{\pi/5, \pi/10, \pi/20, \pi/30\}$ (representing a total number of 16 combinations) (see Section 2.2 for details of probabilistic model and correlation lengths). The impact of different correlation lengths on the radial and angular correlation functions was also presented in Fig. 2.

The elastic properties of the constituent phases and their fluctuation level are summarized in Table 1. The mechanical properties of the deterministic phases were chosen as typical values for silica nanoparticles and polymer matrix [12, 33]. As the elastic properties of the interphase are modeled by the random field introduced in Section 2.2, the fluctuation level was chosen as 40%. Finally, the mean model for the elastic properties of the interphase was chosen to be stiffer than the matrix phase (i.e. $E_{int} = 3/2E_m$), based on the observation that the interphase is a layer of immobilized polymer surrounding the nanofillers [15, 12, 4, 3]. The elasticity tensor of the matrix and the inclusion is presented in Eqs. 18 and 19, respectively.

**Table 1:** Summary of properties of the constituent phases and fluctuation level.

| Parameter | Notation | Unit | Matrix phase | Interphase | Inclusion |
|---|---|---|---|---|---|
| Young's modulus | E | GPa | 1.1 | 1.65 ($3/2E_m$) | 40 |
| Poisson's ratio | $\nu$ | - | 0.4 | 0.4 | 0.25 |
| Bulk modulus | $\kappa$ | GPa | 1.83 | 2.75 | 26.67 |
| Shear modulus | $\mu$ | GPa | 0.39 | 0.59 | 16 |
| Fluctuation level | $\delta$ | % | 0 | 40 | 0 |

$$[C^{\mathrm{m}}] = \begin{bmatrix} 2.36 & 1.57 & 0 \\ 1.57 & 2.36 & 0 \\ 0 & 0 & 0.39 \end{bmatrix}, \tag{18}$$

$$[C^{\mathrm{inc}}] = \begin{bmatrix} 48 & 16 & 0 \\ 16 & 48 & 0 \\ 0 & 0 & 16 \end{bmatrix} \tag{19}$$

### *3.2. Numerical resolution using the finite element method*

The associated homogenization problem (introduced in Section 2.3), formulated with Dirichlet boundary conditions, is solved by the finite element method. An adaptive linear triangular - 1 integration point mesh was used to discretize the domain as shown in

Fig. 4. In this work, about 20 elements in the interphase zone in the radial direction was adopted as optimum (to ensure sampling of the correlation structure of the random field with at least 3 integration points per correlation length [73], which exhibited minimum values of $L_r = h/6$ and $L_\theta = \pi/30$ in the parametric study. Finally, the domain was discretized by a total of 36,349 elements (corresponding to 36,618 degrees of freedom). It should be noted that there were 4,944, 13,713 and 16,692 elements in the inclusion, interphase and matrix phases, respectively.

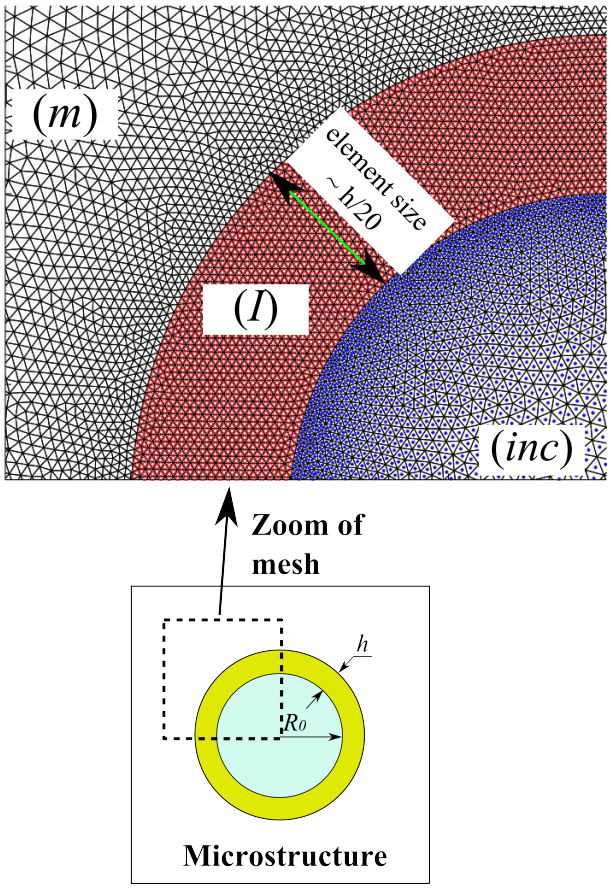


**Fig. 4:** Visualization of finite element mesh for the microstructure.

### *3.3. Micromechanical fields and transmission of force*

This section presents micromechanical fields such as elasticity tensor, strain and stress when applying macroscopic strains as prescribed in Section 2.3. Fig. 6 presents micromechanical fields when applying macroscopic strain in direction $x_2$, while Fig. 7

shows micromechanical fields when applying macroscopic shear strain, for different configurations of correlation lengths: $\{L_r = h,\ L_\theta = \pi/5\}$, $\{L_r = h/6,\ L_\theta = \pi/5\}$, and $\{L_r = h/6,\ L_\theta = \pi/30\}$, respectively. Figs. (6a, 6d and 6g) present a realization for the component $\mathbf{C}_{22}$, while Figs. (7a, 7d and 7g) present a realization for the component $C_{33}$ of the elasticity tensor of the inclusion, interphase, and matrix, for different combinations of correlation lengths: $\{L_r = h,\ L_\theta = \pi/5\}$, $\{L_r = h/6,\ L_\theta = \pi/5\}$, and $\{L_r = h/6,\ L_\theta = \pi/30\}$, respectively. The elastic properties of the interphase were randomly generated associating to the correlation lengths used. For instance, the correlation structure in the interphase radially decreases when $L_r$ decreases from $h$ to $h/6$, as shown in Figs. (6a and 6d) for the component $C_{22}$, and Figs. (7a and 7d) for the component $C_{33}$. Same observation can be made regarding orthoradial correlation structure, as shown in Figs. (6d and 6g) for the component $C_{22}$, and Figs. (7d and 7g) for the component $C_{33}$.

Regarding the local stress field, we can see the role of the inclusion in transferring the load through the domain (i.e. the local stress field in the inclusion could be considered maximal). On the other hand, it is seen that the inclusion is not deformed (i.e. the local strain field in the inclusion is close to zero). We can also see that there is a concentration of stress in the zone of contact between the interphase and inclusion. However, the incidence of the random interphase and its correlation structure on the local strain and stress fields was observed. It is seen in Figs. (6a and 6b) that the poorer the mechanical properties of the interphase compared to the matrix phase, the higher the degree of strain achieved for the same region. The same observation applies in Figs (6d and 6e), Figs (6g and 6h), Figs (7a and 7b), Figs (7d and 7e), Figs (7g and 7h). Consequently, the concentration of stress in the vicinity of the inclusion also depends on the properties of the random interphase and its correlation structure.

Fig. 5 illustrates the ability of the stochastic model to control the change of the elastic properties from isotropic to locally anisotropic in the interphase (under symmetrical positive-definite conditions). The elasticity random field $\left\{[\mathbf{C}^{\text{int}}(\mathbf{x})],\ \mathbf{x} \in (I)\right\}$ in Fig. 5 was controlled by two correlation structures $\{L_r = h/6,\ L_\theta = \pi/5\}$ and fluc-

tuation in the interphase (40% as indicated in Table 1). The mean model $[C^{\text{int}}_{\text{mean}}]$ is also provided to illustrate the anisotropic generation effect. It is seen that the elasticity random field $\{[\mathbf{C}^{\text{int}}(\mathbf{x})],\ \mathbf{x} \in (I)\}$ is locally anisotropic. Finally, an illustration of the spatial fluctuation of the component $C^{\text{int}}_{22}$ is provided.

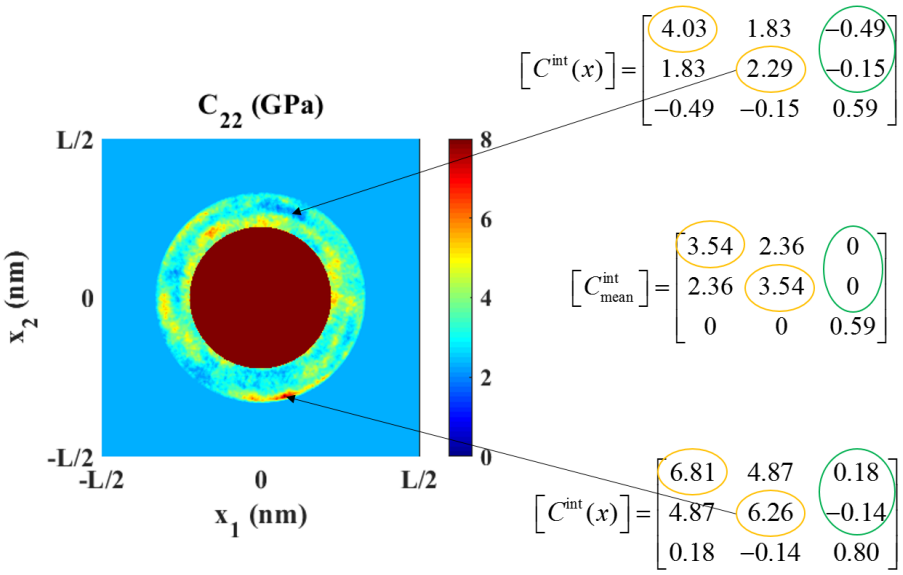


**Fig. 5:** Illustration for anisotropic properties and statistical fluctuation in the interphase: a realization for the elasticity random field $\{[\mathbf{C}^{\text{int}}(\mathbf{x})],\ \mathbf{x} \in (I)\}$ (in GPa) with $\{L_r = h/6,\ L_\theta = \pi/5\}$. The mean model $[C^{\text{int}}_{\text{mean}}]$ is also provided. The elasticity tensor of the matrix and the inclusion is presented in Eqs. 18 and 19, respectively.

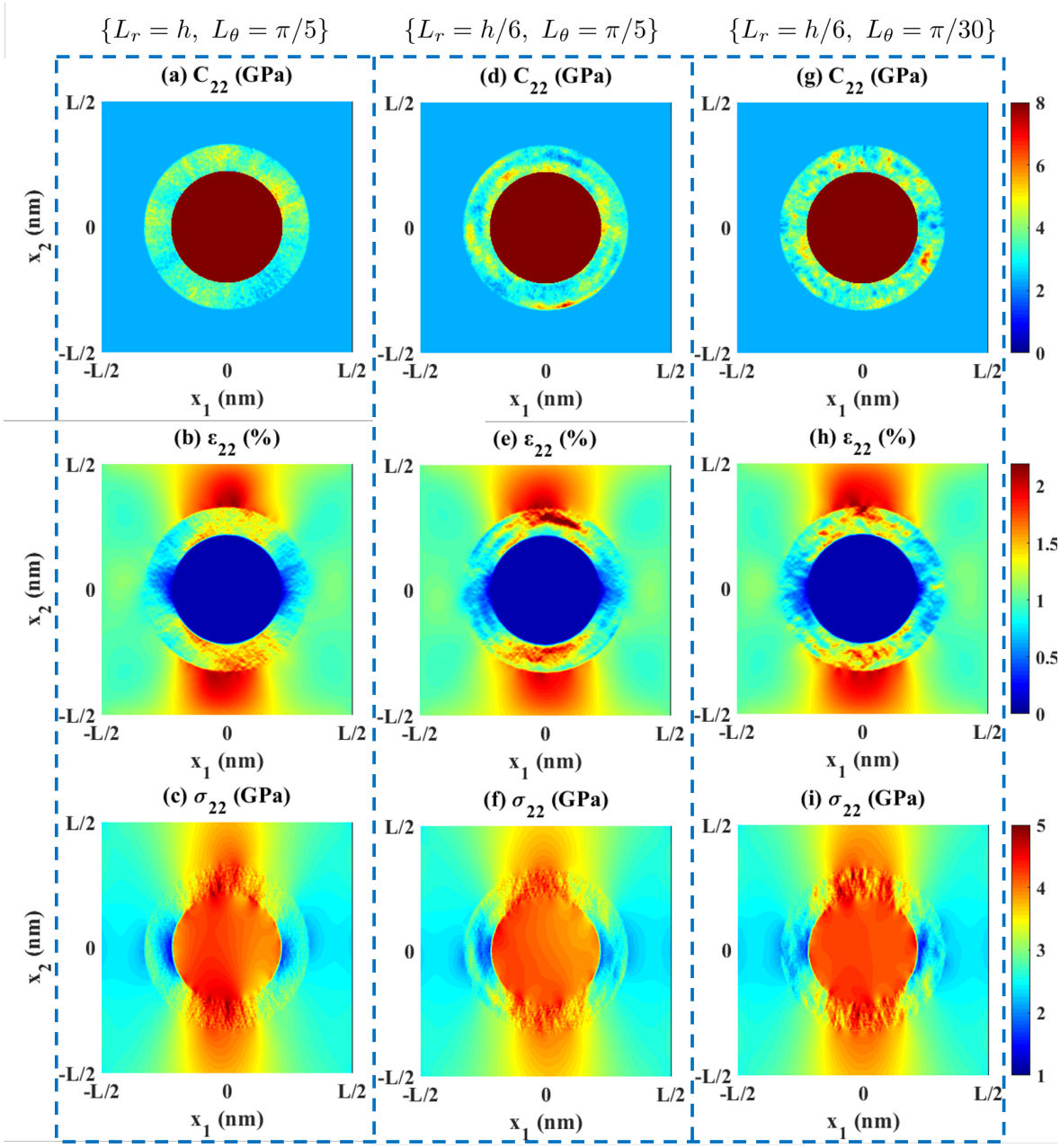


**Fig. 6:** Micromechanical fields when applying macroscopic strain in direction $x_2$ for different configurations of correlation lengths: $\{L_r = h,\ L_\theta = \pi/5\}$, $\{L_r = h/6,\ L_\theta = \pi/5\}$, and $\{L_r = h/6,\ L_\theta = \pi/30\}$: (a, d, g) $C_{22}$ component of the elasticity tensor, (b, e, h) $\varepsilon_{22}$ component of the strain tensor, and (c, f, i) $\sigma_{22}$ component of the stress tensor.

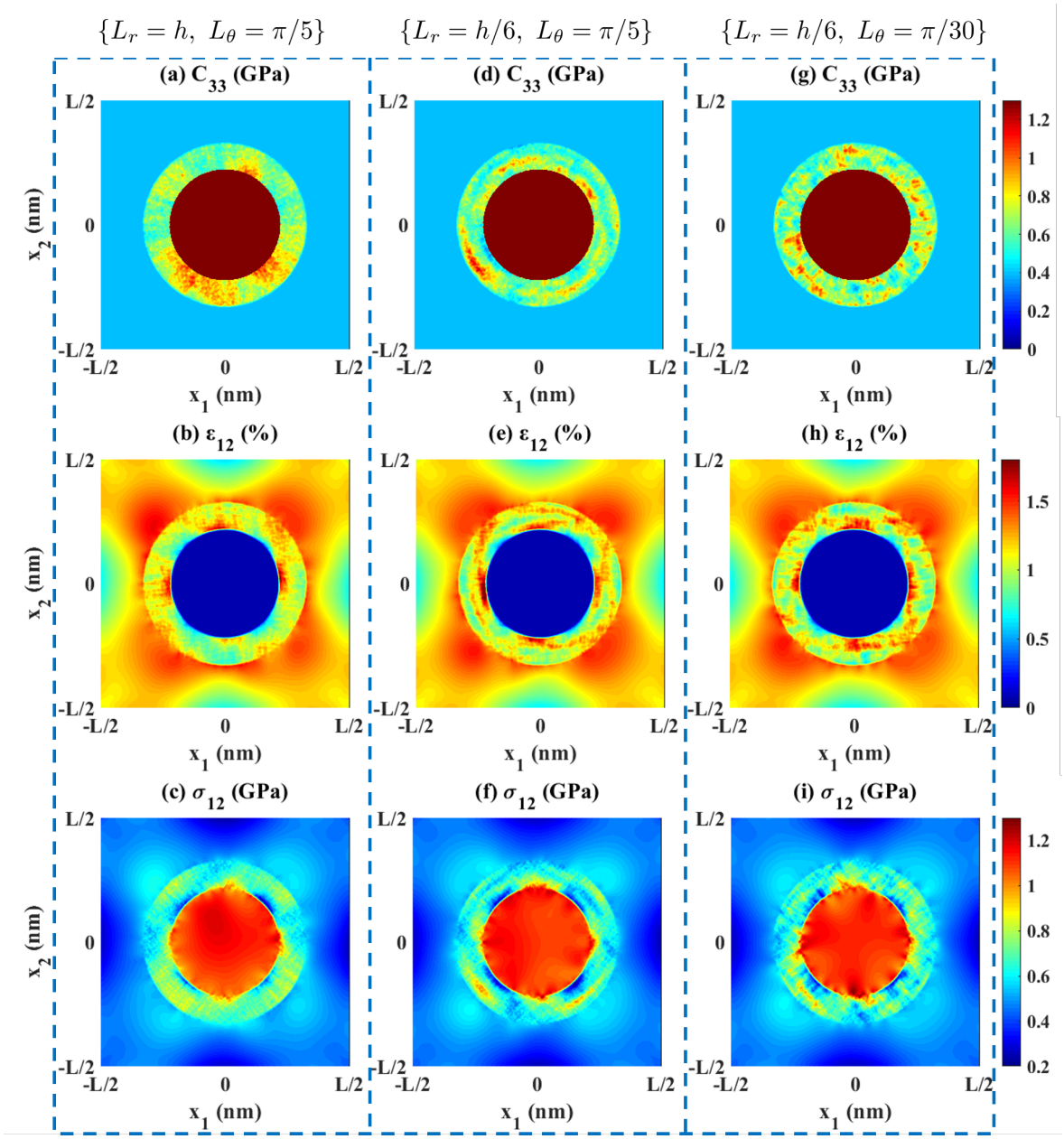


**Fig. 7:** Micromechanical fields when applying macroscopic shear strain for different configurations of correlation lengths: $\{L_r = h,\ L_\theta = \pi/5\}$, $\{L_r = h/6,\ L_\theta = \pi/5\}$, and $\{L_r = h/6,\ L_\theta = \pi/30\}$: (a, d, g) $C_{33}$ component of the elasticity tensor, (b, e, h) $\varepsilon_{12}$ component of the strain tensor, and (c, f, i) $\sigma_{12}$ component of the stress tensor.

### *3.4. Macromechanical properties and statistical convergence*

This section presents the macromechanical properties of the heterogeneous material from a statistical point of view. It should be noted that 2,000 Monte Carlo runs were performed for each combination of correlation structure. The statistical convergence of that number of Monte Carlo runs was estimated by using Eq. 17. Regarding the variation of macromechanical properties as a function of radial correlation length, Figs 8a) and 8c) present the probability distribution of the components $C_{11}^{\text{app}}$ and $C_{33}^{\text{app}}$, respectively, of the apparent elasticity tensor. It is seen that the dispersion of the probability distribution decreases when decreasing the radial correlation length from $L_r = h$ to $L_r = h/6$. However, the average value of the apparent macroscopic properties seems to be unchanged. At the same time, Figs 8b) and 8d) present the statistical convergence for these two components over 2,000 random samples in the interphase region. It is observed that 2,000 Monte Carlo runs was sufficient to obtain statistical convergence for these two components (for all components of the apparent tensor). The same remarks apply when investigating the influence of orthoradial correlation length on the apparent macroscopic properties, as shown in Fig. 8.

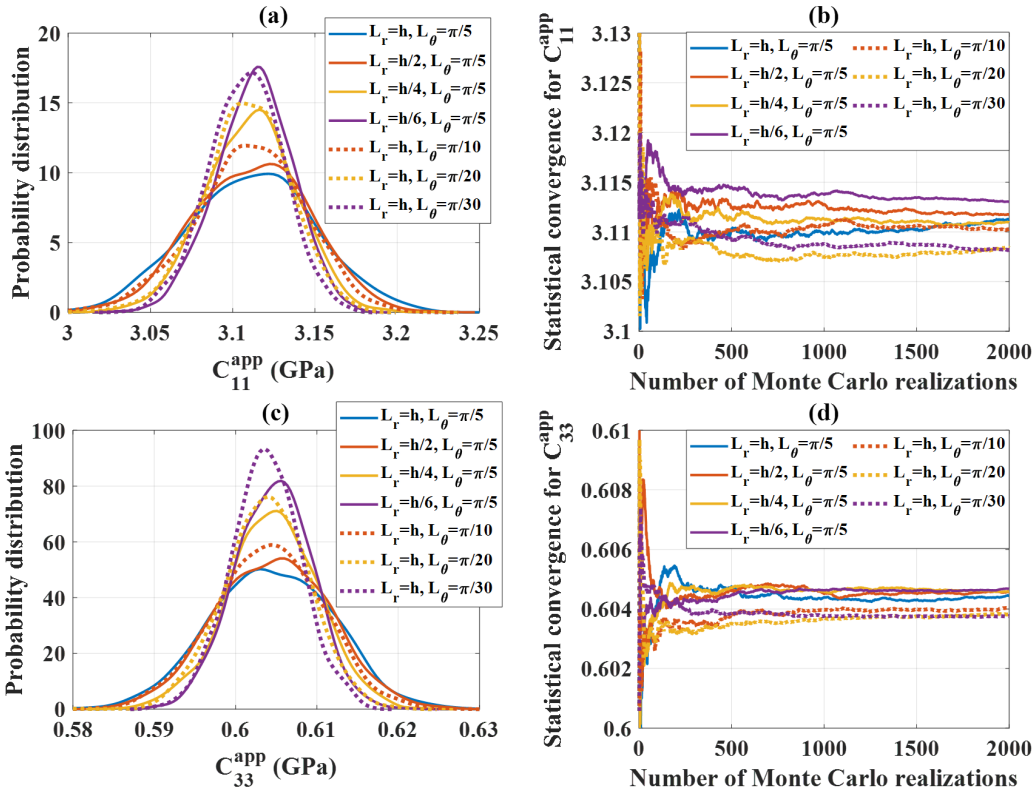


**Fig. 8:** Macromechanical properties of heterogeneous material for different radial and orthoradial correlation lengths: (a) probability distribution of component $C_{11}^{\text{app}}$, (b) statistical convergence of random samples for component $C_{11}^{\text{app}}$, (c) probability distribution of component $C_{33}^{\text{app}}$, (d) statistical convergence of random samples for component $C_{33}^{\text{app}}$.

### *3.5. Parametric analysis of apparent properties*

Fig. 9 presents the coefficients of variation of the random variables $C_{11}^{\text{app}}$ and $C_{33}^{\text{app}}$ for different combinations of correlation lengths. We can see that for a given value of $h$, the coefficients of variation tend towards 0 (for all the components of the apparent tensor) when the correlation lengths tend towards 0. The same remark applies in relation to the coefficient of variation as a function of the orthoradial correlation length $L_\theta$. In other words, when the correlation lengths become small, the fluctuation level in the macroscopic properties tends toward 0. Thus, the hypothesis of separation of scale could be stated for the medium constituting the interphase; such a medium then

becomes homogenizable. It is worth noting that if the statistical fluctuations are non-negligible in the domain, then it is not assumed to be a representative volume element, so that upscaled properties are termed "apparent" (see, for instance, Huet [75] and Ostoja-Starzewski [76]). Therefore, in this case, it is possible to build an equivalent interface model. This point is specifically discussed in the next section.

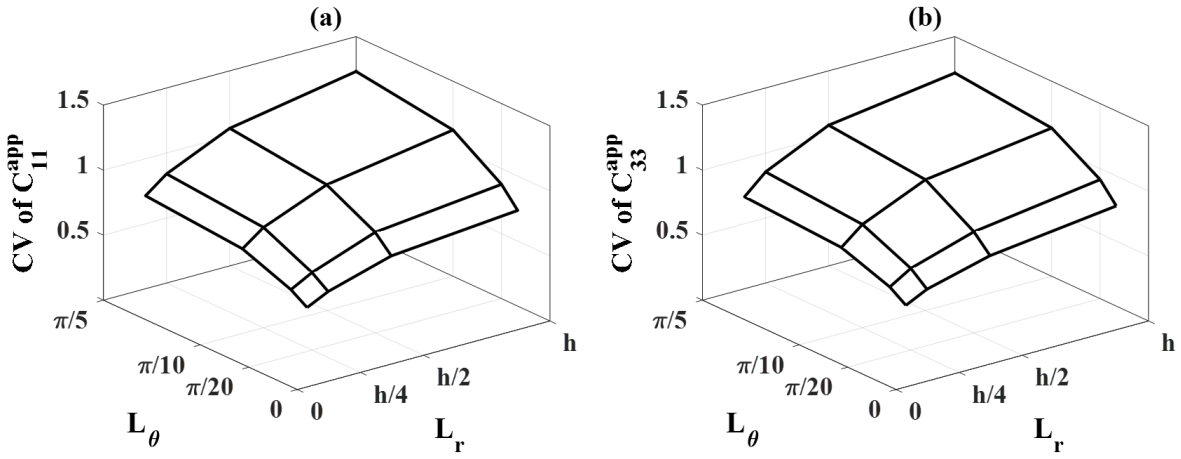


**Fig. 9:** Evolution of the coefficients of variation of (a) $C_{11}^{\text{app}}$ and (b) $C_{33}^{\text{app}}$ depending on parameters $L_r$ and $L_\theta$.

### *3.6. Equivalent interface model*

In this section, we propose to determine the optimal surface properties associated with a coherent imperfect interface model [8, 26], such that the "physical" model (based on stochastic interphase modeling) and the idealized model (based on deterministic modeling using an interface) provide similar estimates (in a sense to be specified) for the effective properties (see Fig. 10a).

Let us first specify the notations. We note $\kappa_{\text{s}}$ and $\mu_{\text{s}}$ for the desired surface properties. For the interface model, the effective properties are estimated by a generalized self-consistent approach (detailed in Lequang and He [8]) and are denoted by $\kappa_{\text{eff}}^{\text{surf}}$ and $\mu_{\text{eff}}^{\text{surf}}$ respectively – note that the effective tensor is, in this case, isotropic. For the model with interphase, for which the apparent tensor presents statistical fluctuations (contained for $L_r \to 0$ and $L_\theta \to 0$), we consider a projection of the average tensor onto

isotropic space [92]:

$$\kappa_{\text{iso}} = \frac{11}{60}(C_{11} + C_{22}) + \frac{19}{30}C_{12} - \frac{1}{15}C_{33} \ , \tag{20}$$

and

$$\mu_{\text{iso}} = \frac{1}{5}(C_{11} + C_{22} + C_{33}) - \frac{2}{5}C_{12} \ . \tag{21}$$

The homogenized model then becomes deterministic and isotropic, characterized by the moduli $\kappa_{\text{iso}}^{\text{int.stoch}}$ and $\mu_{\text{iso}}^{\text{int.stoch}}$. The surface moduli are then deduced by solving the following optimization problem:

$$(\kappa_{\text{s}}, \mu_{\text{s}}) = \underset{\mathbb{R}\text{x}\mathbb{R}}{\arg\min}\, J(\kappa, \mu), \tag{22}$$

where $J$ is the cost function defined by

$$J(\kappa, \mu) = (\kappa_{\text{eff}}^{\text{surf}}(\kappa, \mu) - \kappa_{\text{iso}}^{\text{int.stoch}})^2 + (\mu_{\text{eff}}^{\text{surf}}(\kappa, \mu) - \mu_{\text{iso}}^{\text{int.stoch}})^2. \tag{23}$$

Note, here, that the optimization problem is not formulated with the positivity constraints of elasticity coefficients, in accordance with the literature (see, e.g., [8, 93]). Fig. 10b and Fig. 10c present the results obtained for $\kappa_{\text{s}}$ and $\mu_{\text{s}}$, respectively, for different interphase thicknesses and different inclusion radii. Fig. 10b and Fig. 10c present the results obtained for $\kappa_{\text{s}}$ and $\mu_{\text{s}}$, respectively, for different interphase thicknesses and different inclusion radii. Fig. 10d and Fig. 10e present the results obtained for $\kappa_{\text{s}}$ and $\mu_{\text{s}}$, respectively, as a function of the $h/R_0$ ratio. The interphase-thickness-over-inclusion-radius parameter $h/R_0$ is considered here as a "dimensionless" length-scale parameter.

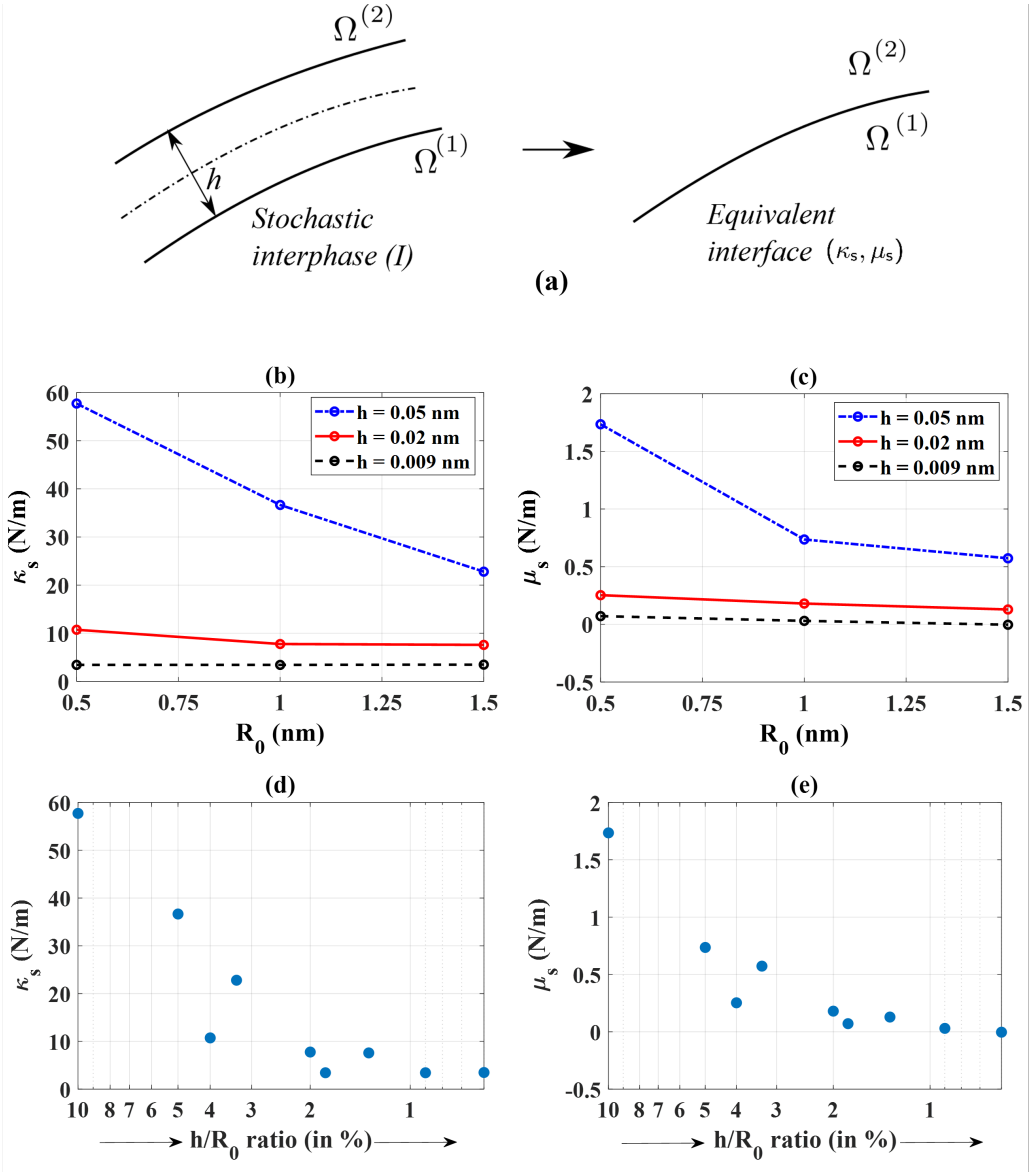


**Fig. 10:** Diagram linking stochastic interphase and equivalent interface model (a); representation of functions: (b) $R_0 \mapsto \kappa_s(R_0)$ and (c) $R_0 \mapsto \mu_s(R_0)$ for different thickness values $h$; and representation of functions: (d) $h/R_0 \mapsto \kappa_s(h/R_0)$ and (e) $h/R_0 \mapsto \mu_s(h/R_0)$.

We find in Fig. 10b and Fig. 10c that when $h$ is too large, the surface moduli depend strongly on the radius $R_0$ of the inclusion. This is due to the fact that in this case, the interphase cannot be relevantly modeled by an equivalent interface. When the thickness decreases and for sufficiently short correlation lengths, the interface properties become

almost independent of the radius of the inclusion. This observation is consistent with the homogenization theories [30, 9]. Thus, the hypothesis of modeling the interphase by an equivalent interface becomes admissible. The bridge between interphase and interface models is, at least, possible where the interphase thickness is sufficiently small. The same remarks apply regarding the interphase properties as a function of $h/R_0$ in Fig. 10d and Fig. 10e. For a given inclusion volume fraction, the interphase-thickness-over-inclusion-radius plays a crucial role. Moreover, Fig. 10d and Fig. 10e show that the modeling of the stochastic interphase by an equivalent interface becomes admissible when the "dimensionless" length-scale parameter $h/R_0$ is smaller than 2%.

The probabilistic model (with finite-volume interphase) can provide different homogenized responses when the actual size of the inclusion changes. This effect is mainly due to the increase of the interphase volume fraction in the microstructure when the size of the inclusion decreases, for a given inclusion volume fraction. Such a positive effect of interphase volume fraction on the elastic modulus of nanocomposites is consistent with thee numerical investigation by Zakaria and Shelesh-Nezhad [48], who compared FEM and Odegard's Equivalent Interface Model [35]. However, the current probabilistic interphase model, used in conjunction with classical homogenization principles, is still limited and needs to be improved in order to more clearly reflect the size-dependent effect when the inclusion characteristic size enters the nanometric scale. For a comparison with the coherent interface model, we have first evaluated the hypothesis of separation of scale in the interphase medium, as a function of the correlation structures. Secondly, the results obtained in Fig. 10 show that the bridge between interphase and interface models is, at least, possible where the interphase thickness is sufficiently small, identified as being 2% max. for the "dimensionless" length-scale parameter $h/R_0$. Despite the aforesaid efforts, a more efficient homogenization scheme needs to be developed to take account of the size-dependent effect, from both the physical and numerical points of view. The classical homogenization framework could be extended to incorporate the size-dependent effect by introducing an incremental energy equivalence (see Firooz et al. [16] for an extension of the composite sphere assemblage model). From a numerical

point view, two approaches could be indicated: (i) standard FEM with surface element (see Gao Wei et al. [94], Javili et al. [55], Firooz et al. [16]), and (ii) eXtended FEM with the level set method (see Yvonnet et al. [9], Farsad et al. [95], Ren et al. [96] , Dang et al. [97]). Last but not least, the classical homogenization principles can also be used if an equivalent inclusion that substitutes the inclusion-plus-interphase is employed [57, 16, 98, 99].

## 4. Conclusion and outlook

In this work, we are interested in the modeling of heterogeneous materials presenting surface effects. To do this, we relied on probabilistic modeling of the interphase zone, the existence of which is highlighted in the literature. First, we produced a probabilistic model of the elastic properties of the interphase, modeled by a random field with matrix values. We then proceeded to propagate the uncertainties in order to estimate the apparent elastic properties of the microstructure. Parametric analysis highlighted the role of the lengths of radial and orthoradial correlations for the homogenization of the properties of the interphase. Secondly, we characterized an equivalent interface model, for which the surface moduli are obtained by the resolution of an optimization problem formulated on the basis of the effective properties. It is observed that when the thickness of the interphase is sufficiently small, the surface properties obtained become independent of the radius of the inclusion.

The proposed research methodology in this study can be extended to finite deformations and non-linear elasticity. Firstly, the random field model of the interphase elasticity tensor can be applied to any uncertain random materials exhibiting spatial fluctuations. Thus, from a computational point of view, the stochastic model presented in this study can be readily coupled with iterative techniques (e.g. the arc-length method [100], the Newton–Raphson technique [101, 102], or normal flow [103]) for solving large deformation problems. For instance, in Ref. [102], the authors constructed a probabilistic model for the random elasticity tensor, and deduced the influence of such fluctuation on the macroscopic behavior of the structural member in buckling

failure (large displacement when the load increment is small). Secondly, the construction of stochastic models for random strain energy functions, recently presented in [104, 105, 106], shows that probabilistic random field modeling can be applied to non-linear elasticity. Staber et al. [104] developed a stochastic model for the hyperelastic strain energy function for laminated composites, and then identified model parameters using an experimental database. More works dealing with stochastic modeling for non-linear heterogeneous materials can be found in [107, 64, 108, 109, 110, 73].

In further studies, a fully probabilistic model considering the interphase thickness to be a random variable should be developed. Such a view is more closely in keeping with the random elastic properties in the interphase zone. The interphase thickness could also be considered as an unknown parameter that could be determined probabilistically by coupling the stochastic model and, for instance, results obtained from Molecular Dynamics simulations.


## Acknowledgment

The authors would like to thank Prof. J. Guilleminot (Duke University, Durham, USA), and Prof. C. Soize (Université Paris-Est, Marne-la-Vallée, France), for their helpful advice and comments on this paper.

## Funding

This research did not receive any specific grant from funding agencies in the public, commercial, or not-for-profit sectors.


## Conflict of Interest

The authors declare that there is no conflict of interest.

## Data availability

The raw/processed data required to reproduce these findings will be made available on request.

## References


[1] P. M. Ajayan, L. S. Schadler, P. V. Braun, P. Keblinski, Nanocomposite Science and Technology, Wiley-VCH Verlag GmbH, Weinheim; Chichester, 2015.

[2] K. W. Putz, M. J. Palmeri, R. B. Cohn, R. Andrews, L. C. Brinson, Effect of Cross-Link Density on Interphase Creation in Polymer Nanocomposites, Macromolecules 41 (18) (2008) 6752–6756. doi:10.1021/ma800830p.

[3] A. Papon, K. Saalwächter, K. Schäler, L. Guy, F. Lequeux, H. Montes, Low-Field NMR Investigations of Nanocomposites: Polymer Dynamics and Network Effects, Macromolecules 44 (4) (2011) 913–922. doi:10.1021/ma102486x.

[4] S. E. Harton, S. K. Kumar, H. Yang, T. Koga, K. Hicks, H. Lee, J. Mijovic, M. Liu, R. S. Vallery, D. W. Gidley, Immobilized Polymer Layers on Spherical Nanoparticles, Macromolecules 43 (7) (2010) 3415–3421. doi:10.1021/ma902484d.

[5] I. Chung, M. Cho, Recent Studies on the Multiscale Analysis of Polymer Nanocomposites, Multiscale Science and Engineering 1 (3) (2019) 167–195. doi:10.1007/s42493-019-00022-4.

[6] M.-T. Hoang, J. Yvonnet, A. Mitrushchenkov, G. Chambaud, First-principles based multiscale model of piezoelectric nanowires with surface effects, Journal of Applied Physics 113 (1) (2013) 014309. doi:10.1063/1.4773333.

[7] J. Yvonnet, H. Le-Quang, C. Toulemonde, Q.-C. He, Thermo-mechanical modelling of materials containing micro/nano inclusions with imperfect interfaces, International Journal of Material Forming 1 (1) (2008) 1139–1142. doi:10.1007/s12289-008-0181-2.

[8] H. L. Quang, Q. C. He, Size-dependent effective thermoelastic properties of nanocomposites with spherically anisotropic phases, Journal of the Mechanics and Physics of Solids 55 (9) (2007) 1899–1931. doi:10.1016/j.jmps.2007.02.005.

[9] J. Yvonnet, H. L. Quang, Q. C. He, An XFEM/level set approach to modelling surface/interface effects and to computing the size-dependent effective properties of nanocomposites, Computational Mechanics 42 (1) (2008) 119–131. doi:10.1007/s00466-008-0241-y.

[10] J. Berriot, F. Lequeux, L. Monnerie, H. Montes, D. Long, P. Sotta, Filler–elastomer interaction in model filled rubbers, a 1H NMR study, Journal of Non-Crystalline Solids 307-310 (2002) 719–724. doi:10.1016/S0022-3093(02)01552-1.

[11] E. Monteiro, Q. C. He, J. Yvonnet, Hyperelastic large deformations of two-phase composites with membrane-type interface, International Journal of Engineering Science 49 (9) (2011) 985–1000. doi:10.1016/j.ijengsci.2011.05.011.

[12] D. Brown, V. Marcadon, P. Mélé, N. D. Albérola, Effect of Filler Particle Size on the Properties of Model Nanocomposites, Macromolecules 41 (4) (2008) 1499–1511. doi:10.1021/ma701940j.

[13] J. Choi, S. Yang, S. Yu, H. Shin, M. Cho, Method of scale bridging for thermoelasticity of cross-linked epoxy/SiC nanocomposites at a wide range of temperatures, Polymer 53 (22) (2012) 5178–5189. doi:10.1016/j.polymer.2012.08.041.

[14] H. Shin, S. Yang, J. Choi, S. Chang, M. Cho, Effect of interphase percolation on mechanical behavior of nanoparticle-reinforced polymer nanocomposite with filler agglomeration: A multiscale approach, Chemical Physics Letters 635 (2015) 80–85. doi:10.1016/j.cplett.2015.06.054.

[15] A. Ghanbari, T. V. M. Ndoro, F. Leroy, M. Rahimi, M. C. Böhm, F. Müller-Plathe, Interphase Structure in Silica–Polystyrene Nanocomposites: A Coarse-Grained Molecular Dynamics Study, Macromolecules 45 (1) (2012) 572–584. doi:10.1021/ma202044e.

[16] S. Firooz, G. Chatzigeorgiou, F. Meraghni, A. Javili, Homogenization accounting for size effects in particulate composites due to general interfaces, Mechanics of Materials 139 (2019) 103204. doi:10.1016/j.mechmat.2019.103204.

[17] E. Hervé-Luanco, Elastic behavior of composites containing multi-layer coated particles with imperfect interface bonding conditions and application to size effects and mismatch in these composites, International Journal of Solids and Structures 51 (15) (2014) 2865–2877. doi:10.1016/j.ijsolstr.2014.04.008.

[18] S. Firooz, A. Javili, Understanding the role of general interfaces in the overall behavior of composites and size effects, Computational Materials Science 162 (2019) 245–254. doi:10.1016/j.commatsci.2019.02.042.

[19] Z. Yao, Z.-M. Huang, Stress concentration factors in the matrix with different imperfect interfaces, International Journal of Damage Mechanics 23 (6) (2014) 745–771. doi:10.1177/1056789513512345.

[20] H. Dong, J. Wang, M. B. Rubin, Cosserat interphase models for elasticity with application to the interphase bonding a spherical inclusion to an infinite matrix, International Journal of Solids and Structures 51 (2) (2014) 462–477. doi:10.1016/j.ijsolstr.2013.10.020.

[21] M. E. Gurtin, A. I. Murdoch, A continuum theory of elastic material surfaces, Archive for Rational Mechanics and Analysis 57 (1975) 291–323. doi:10.1007/BF00261375.

[22] M. E. Gurtin, J. Weissmüller, F. Larché, A general theory of curved deformable interfaces in solids at equilibrium, Philosophical Magazine A 78 (5) (1998) 1093–1109. doi:10.1080/01418619808239977.

[23] B. J. Yang, Y. Y. Hwang, H. K. Lee, Elastoplastic modeling of polymeric composites containing randomly located nanoparticles with an interface effect, Composite Structures 99 (2013) 123–130. doi:10.1016/j.compstruct.2012.11.043.

[24] L. Nazarenko, H. Stolarski, H. Altenbach, Effective properties of short-fiber composites with Gurtin-Murdoch model of interphase, International Journal of Solids and Structures 97-98 (2016) 75–88. doi:10.1016/j.ijsolstr.2016.07.041.

[25] G. Chatzigeorgiou, F. Meraghni, A. Javili, Generalized interfacial energy and size effects in composites, Journal of the Mechanics and Physics of Solids 106 (2017) 257–282. doi:10.1016/j.jmps.2017.06.002.

[26] H. L. Quang, Q. C. He, Variational principles and bounds for elastic inhomogeneous materials with coherent imperfect interfaces, Mechanics of Materials 40 (10) (2008) 865–884. doi:10.1016/j.mechmat.2008.04.003.

[27] Y. Benveniste, A general interface model for a three-dimensional curved thin anisotropic interphase between two anisotropic media, Journal of the Mechanics and Physics of Solids 54 (4) (2006) 708–734. doi:10.1016/j.jmps.2005.10.009.

[28] S. Brisard, L. Dormieux, D. Kondo, Hashin–Shtrikman bounds on the bulk modulus of a nanocomposite with spherical inclusions and interface effects, Computational Materials Science 48 (3) (2010) 589–596. doi:10.1016/j.commatsci.2010.02.027.

[29] H. L. Duan, J. Wang, Z. P. Huang, B. L. Karihaloo, Size-dependent effective elastic constants of solids containing nano-inhomogeneities with interface stress, Journal of the Mechanics and Physics of Solids 53 (7) (2005) 1574–1596. doi:10.1016/j.jmps.2005.02.009.

[30] J. Wang, H. L. Duan, Z. Zhang, Z. P. Huang, An anti-interpenetration model and connections between interphase and interface models in particle-reinforced composites, International Journal of Mechanical Sciences 47 (4) (2005) 701–718. doi:10.1016/j.ijmecsci.2004.12.014.

[31] B. Kim, J. Choi, S. Yang, S. Yu, M. Cho, Multiscale modeling of interphase in

crosslinked epoxy nanocomposites, Composites Part B: Engineering 120 (2017) 128–142. doi:10.1016/j.compositesb.2017.03.059.

[32] J. Choi, H. Shin, S. Yang, M. Cho, The influence of nanoparticle size on the mechanical properties of polymer nanocomposites and the associated interphase region: A multiscale approach, Composite Structures 119 (2015) 365–376. doi:10.1016/j.compstruct.2014.09.014.

[33] V. Marcadon, D. Brown, E. Hervé, P. Mélé, N. D. Albérola, A. Zaoui, Confrontation between Molecular Dynamics and micromechanical approaches to investigate particle size effects on the mechanical behaviour of polymer nanocomposites, Computational Materials Science 79 (2013) 495–505. doi:10.1016/j.commatsci.2013.07.002.

[34] B. Paliwal, M. Cherkaoui, Estimation of anisotropic elastic properties of nanocomposites using atomistic-continuum interphase model, International Journal of Solids and Structures 49 (18) (2012) 2424–2438. doi:10.1016/j.ijsolstr.2012.05.004.

[35] G. M. Odegard, T. C. Clancy, T. S. Gates, Modeling of the mechanical properties of nanoparticle/polymer composites, Polymer 46 (2) (2005) 553–562. doi:10.1016/j.polymer.2004.11.022.

[36] S. Chang, S. Yang, H. Shin, M. Cho, Multiscale homogenization model for thermoelastic behavior of epoxy-based composites with polydisperse SiC nanoparticles, Composite Structures 128 (2015) 342–353. doi:10.1016/j.compstruct.2015.03.041.

[37] H. Le-Quang, G. Bonnet, Q.-C. He, Size-dependent Eshelby tensor fields and effective conductivity of composites made of anisotropic phases with highly conducting imperfect interfaces, Physical Review B 81 (6) (2010) 064203. doi:10.1103/PhysRevB.81.064203.

[38] H. Le Quang, T. L. Phan, G. Bonnet, Effective thermal conductivity of periodic composites with highly conducting imperfect interfaces, International Journal of Thermal Sciences 50 (8) (2011) 1428–1444. doi:10.1016/j.ijthermalsci.2011.03.009.

[39] R. D. Peng, H. W. Zhou, H. W. Wang, L. Mishnaevsky, Modeling of nano-reinforced polymer composites: Microstructure effect on Young's modulus, Computational Materials Science 60 (2012) 19–31. doi:10.1016/j.commatsci.2012.03.010.

[40] K. Baek, H. Shin, T. Yoo, M. Cho, Two-step multiscale homogenization for mechanical behaviour of polymeric nanocomposites with nanoparticulate agglomerations, Composites Science and Technology 179 (2019) 97–105. doi:10.1016/j.compscitech.2019.05.006.

[41] T. T. Le, J. Guilleminot, C. Soize, Stochastic continuum modeling of random interphases from atomistic simulations. Application to a polymer nanocomposite, Computer Methods in Applied Mechanics and Engineering 303 (2016) 430–449. doi:10.1016/j.cma.2015.10.006.

[42] A. Z. Zakaria, K. Shelesh-Nezhad, The Effects of Interphase and Interface Characteristics on the Tensile Behaviour of POM/CaCO3 Nanocomposites:, Nanomaterials and Nanotechnology (Jan. 2014). doi:10.5772/58696.

[43] D. Ciprari, K. Jacob, R. Tannenbaum, Characterization of Polymer Nanocomposite Interphase and Its Impact on Mechanical Properties, Macromolecules 39 (19) (2006) 6565–6573. doi:10.1021/ma0602270.

[44] R. A. Riggleman, G. Toepperwein, G. J. Papakonstantopoulos, J.-L. Barrat, J. J. de Pablo, Entanglement network in nanoparticle reinforced polymers, The Journal of Chemical Physics 130 (24) (2009) 244903. doi:10.1063/1.3148026.

[45] T. V. M. Ndoro, M. C. Böhm, F. Müller-Plathe, Interface and Interphase Dynamics of Polystyrene Chains near Grafted and Ungrafted Silica Nanoparticles, Macromolecules 45 (1) (2012) 171–179. doi:10.1021/ma2020613.

[46] M. Vacatello, Monte Carlo Simulations of Polymer Melts Filled with Solid Nanoparticles, Macromolecules 34 (6) (2001) 1946–1952. doi:10.1021/ma0015370.

[47] T. Chen, H.-J. Qian, Y.-L. Zhu, Z.-Y. Lu, Structure and Dynamics Properties at Interphase Region in the Composite of Polystyrene and Cross-Linked Polystyrene Soft Nanoparticle, Macromolecules 48 (8) (2015) 2751–2760. doi:10.1021/ma502383n.

[48] A. Zamani Zakaria, K. Shelesh-Nezhad, Quantifying the particle size and interphase percolation effects on the elastic performance of semi-crystalline nanocomposites, Computational Materials Science 117 (2016) 502–510. doi:10.1016/j.commatsci.2016.02.026.

[49] S. Ma, I. Scheider, S. Bargmann, Ultrastrong nanocomposites with interphases: Nonlocal deformation and damage behavior, European Journal of Mechanics - A/Solids 75 (2019) 93–108. doi:10.1016/j.euromechsol.2019.01.011.

[50] H. Zolfaghari, M. Silani, V. Yaghoubi, M. Jamshidian, A. M. Hamouda, Stochastic analysis of interphase effects on elastic modulus and yield strength of nylon 6/clay nanocomposites, International Journal of Mechanics and Materials in Design 15 (1) (2019) 109–123. doi:10.1007/s10999-017-9399-9.

[51] N. Vu-Bac, M. Silani, T. Lahmer, X. Zhuang, T. Rabczuk, A unified framework for stochastic predictions of mechanical properties of polymeric nanocomposites, Computational Materials Science 96 (2015) 520–535. doi:10.1016/j.commatsci.2014.04.066.

[52] A. Nouy, A. Clément, eXtended Stochastic Finite Element Method for the numerical simulation of heterogeneous materials with random material interfaces, International Journal for Numerical Methods in Engineering 83 (10) (2010) 1312–1344. doi:10.1002/nme.2865.

[53] K. Sab, B. Nedjar, Periodization of random media and representative volume element size for linear composites, Comptes Rendus Mécanique 333 (2) (2005) 187–195. doi:10.1016/j.crme.2004.10.003.

[54] V.-P. Tran, J. Guilleminot, S. Brisard, K. Sab, Stochastic modeling of mesoscopic elasticity random field, Mechanics of Materials 93 (2016) 1–12. doi:10.1016/j.mechmat.2015.10.007.

[55] A. Javili, P. Steinmann, J. Mosler, Micro-to-macro transition accounting for general imperfect interfaces, Computer Methods in Applied Mechanics and Engineering 317 (2017) 274–317. doi:10.1016/j.cma.2016.12.025.

[56] Z. Hashin, Thin interphase/imperfect interface in elasticity with application to coated fiber composites, Journal of the Mechanics and Physics of Solids 50 (12) (2002) 2509–2537. doi:10.1016/S0022-5096(02)00050-9.

[57] S. T. Gu, J. T. Liu, Q. C. He, Size-dependent effective elastic moduli of particulate composites with interfacial displacement and traction discontinuities, International Journal of Solids and Structures 51 (13) (2014) 2283–2296. doi:10.1016/j.ijsolstr.2014.02.033.

[58] G. Chatzigeorgiou, A. Javili, P. Steinmann, Multiscale modelling for composites with energetic interfaces at the micro- or nanoscale:, Mathematics and Mechanics of Solids (Dec. 2013). doi:10.1177/1081286513516122.

[59] E. Voyiatzis, M. Rahimi, F. Müller-Plathe, M. C. Böhm, How Thick Is the Polymer Interphase in Nanocomposites? Probing It by Local Stress Anisotropy

and Gas Solubility, Macromolecules 47 (22) (2014) 7878–7889. doi:10.1021/ma500556q.

[60] D. Brown, P. Mélé, S. Marceau, N. D. Albérola, A Molecular Dynamics Study of a Model Nanoparticle Embedded in a Polymer Matrix, Macromolecules 36 (4) (2003) 1395–1406. doi:10.1021/ma020951s.

[61] J. Guilleminot, C. Soize, D. Kondo, Mesoscale probabilistic models for the elasticity tensor of fiber reinforced composites: Experimental identification and numerical aspects, Mechanics of Materials 41 (12) (2009) 1309–1322. doi:10.1016/j.mechmat.2009.08.004.

[62] J. Guilleminot, C. Soize, D. Kondo, C. Binetruy, Theoretical framework and experimental procedure for modelling mesoscopic volume fraction stochastic fluctuations in fiber reinforced composites, International Journal of Solids and Structures 45 (21) (2008) 5567–5583. doi:10.1016/j.ijsolstr.2008.06.002.

[63] M. T. Nguyen, C. Desceliers, C. Soize, J. M. Allain, H. Gharbi, MULTISCALE IDENTIFICATION OF THE RANDOM ELASTICITY FIELD AT MESOSCALE OF A HETEROGENEOUS MICROSTRUCTURE USING MULTISCALE EXPERIMENTAL OBSERVATIONS, International Journal for Multiscale Computational Engineering 13 (4) (2015). doi:10.1615/IntJMultCompEng.2015011435.

[64] A. Clément, C. Soize, J. Yvonnet, Uncertainty quantification in computational stochastic multiscale analysis of nonlinear elastic materials, Computer Methods in Applied Mechanics and Engineering 254 (2013) 61–82. doi:10.1016/j.cma.2012.10.016.

[65] J. Guilleminot, C. Soize, A stochastic model for elasticity tensors with uncertain material symmetries, International Journal of Solids and Structures 47 (22) (2010) 3121–3130. doi:10.1016/j.ijsolstr.2010.07.013.

[66] J. Guilleminot, A. Noshadravan, C. Soize, R. G. Ghanem, A probabilistic model for bounded elasticity tensor random fields with application to polycrystalline microstructures, Computer Methods in Applied Mechanics and Engineering 200 (17) (2011) 1637–1648. doi:10.1016/j.cma.2011.01.016.

[67] C. Soize, Non-Gaussian positive-definite matrix-valued random fields for elliptic stochastic partial differential operators, Computer Methods in Applied Mechanics and Engineering 195 (1) (2006) 26–64. doi:10.1016/j.cma.2004.12.014.

[68] E. T. Jaynes, Information Theory and Statistical Mechanics, Physical Review 106 (4) (1957) 620–630. doi:10.1103/PhysRev.106.620.

[69] C. E. Shannon, A Mathematical Theory of Communication, Bell System Technical Journal 27 (3) (1948) 379–423. doi:10.1002/j.1538-7305.1948.tb01338.x.

[70] C. Soize, A nonparametric model of random uncertainties for reduced matrix models in structural dynamics, Probabilistic Engineering Mechanics 15 (3) (2000) 277–294. doi:10.1016/S0266-8920(99)00028-4.

[71] C. Soize, C. Desceliers, J. Guilleminot, T.-T. Le, M.-T. Nguyen, G. Perrin, J.-M. Allain, H. Gharbi, D. Duhamel, C. Funfschilling, Stochastic representations and statistical inverse identification for uncertainty quantification in computational mechanics, in: UNCECOMP 2015, 1st ECCOMAS Thematic International Conference on Uncertainty Quantification in Computational Sciences and Engineering, 2015, pp. 1–26.

[72] J. Guilleminot, C. Soize, Stochastic Model and Generator for Random Fields with Symmetry Properties: Application to the Mesoscopic Modeling of Elastic Random Media, Multiscale Modeling & Simulation 11 (3) (2013) 840–870. doi:10.1137/120898346.

[73] C. Soize, Tensor-valued random fields for meso-scale stochastic model of anisotropic elastic microstructure and probabilistic analysis of representative vol-

ume element size, Probabilistic Engineering Mechanics 23 (2) (2008) 307–323. doi:10.1016/j.probengmech.2007.12.019.

[74] V. Dubourg, B. Sudret, M. Cazuguel, Modélisation probabiliste de champs d'imperfections géométriques de coques résistantes de sous-marins, in: 10e Colloque National En Calcul Des Structures, Giens, France, 2011, p. Clé USB.

[75] C. Huet, Application of variational concepts to size effects in elastic heterogeneous bodies, Journal of the Mechanics and Physics of Solids 38 (6) (1990) 813–841. doi:10.1016/0022-5096(90)90041-2.

[76] M. Ostoja-Starzewski, Material spatial randomness: From statistical to representative volume element, Probabilistic Engineering Mechanics 21 (2) (2006) 112–132. doi:10.1016/j.probengmech.2005.07.007.

[77] T. Kanit, S. Forest, I. Galliet, V. Mounoury, D. Jeulin, Determination of the size of the representative volume element for random composites: Statistical and numerical approach, International Journal of Solids and Structures 40 (13) (2003) 3647–3679. doi:10.1016/S0020-7683(03)00143-4.

[78] M. Ostoja-Starzewski, Micromechanics as a basis of random elastic continuum approximations, Probabilistic Engineering Mechanics 8 (2) (1993) 107–114. doi:10.1016/0266-8920(93)90004-F.

[79] J. Guilleminot, T. T. Le, C. Soize, Stochastic framework for modeling the linear apparent behavior of complex materials: Application to random porous materials with interphases, Acta Mechanica Sinica 29 (6) (2013) 773–782. doi:10.1007/s10409-013-0101-7.

[80] M. Chevreuil, A. Nouy, E. Safatly, A multiscale method with patch for the solution of stochastic partial differential equations with localized uncertainties, Computer Methods in Applied Mechanics and Engineering 255 (2013) 255–274. doi:10.1016/j.cma.2012.12.003.

[81] H. Le Quang, H. T. Le, D. H. Nguyen, Q. C. He, Two-scale homogenization of elastic layered composites with interfaces oscillating in two directions, Mechanics of Materials 75 (2014) 60–72. doi:10.1016/j.mechmat.2014.04.002.

[82] H. T. Le, H. Le Quang, Q. C. He, The effective elastic moduli of columnar composites made of cylindrically anisotropic phases with rough interfaces, International Journal of Solids and Structures 51 (14) (2014) 2633–2647. doi:10.1016/j.ijsolstr.2014.03.036.

[83] H. L. Quang, Q. C. He, A one-parameter generalized self-consistent model for isotropic multiphase composites, International Journal of Solids and Structures 44 (21) (2007) 6805–6825. doi:10.1016/j.ijsolstr.2007.03.008.

[84] T.-T. Le, Modélisation stochastique, en mécanique des milieux continus, de l'interphase inclusion-matrice à partir de simulations en dynamique moléculaire, PhD Thesis, University of Paris-Est Marne-la-Vallée, Paris, France (Oct. 2015).

[85] D. V. Dao, H. Adeli, H.-B. Ly, L. M. Le, V. M. Le, T.-T. Le, B. T. Pham, A Sensitivity and Robustness Analysis of GPR and ANN for High-Performance Concrete Compressive Strength Prediction Using a Monte Carlo Simulation, Sustainability 12 (3) (2020) 830. doi:10.3390/su12030830.

[86] H.-B. Ly, B. T. Pham, L. M. Le, T.-T. Le, V. M. Le, P. G. Asteris, Estimation of axial load-carrying capacity of concrete-filled steel tubes using surrogate models, Neural Computing and Applications (Jul. 2020). doi:10.1007/s00521-020-05214-w.

[87] T.-T. Le, Surrogate Neural Network Model for Prediction of Load-Bearing Capacity of CFSS Members Considering Loading Eccentricity, Applied Sciences 10 (10) (2020) 3452. doi:10.3390/app10103452.

[88] M. D. Nguyen, B. T. Pham, L. S. Ho, H.-B. Ly, T.-T. Le, C. Qi, V. M. Le, L. M. Le, I. Prakash, L. H. Son, D. T. Bui, Soft-computing techniques for prediction

of soils consolidation coefficient, CATENA 195 (2020) 104802. doi:10.1016/j.catena.2020.104802.

[89] D. V. Dao, H.-B. Ly, H.-L. T. Vu, T.-T. Le, B. T. Pham, Investigation and Optimization of the C-ANN Structure in Predicting the Compressive Strength of Foamed Concrete, Materials 13 (5) (2020) 1072. doi:10.3390/ma13051072.

[90] S. Yu, S. Yang, M. Cho, Multi-scale modeling of cross-linked epoxy nanocomposites, Polymer 50 (3) (2009) 945–952. doi:10.1016/j.polymer.2008.11.054.

[91] J.-L. Tsai, S.-H. Tzeng, Characterizing Mechanical Properties of Particulate Nanocomposites Using Micromechanical Approach:, Journal of Composite Materials (Aug. 2008). doi:10.1177/0021998308095503.

[92] J. Guilleminot, C. Soize, Probabilistic modeling of apparent tensors in elastostatics: A MaxEnt approach under material symmetry and stochastic boundedness constraints, Probabilistic Engineering Mechanics 28 (2012) 118–124. doi:10.1016/j.probengmech.2011.07.004.

[93] R. E. Miller, V. B. Shenoy, Size-dependent elastic properties of nanosized structural elements, Nanotechnology 11 (3) (2000) 139–147. doi:10.1088/0957-4484/11/3/301.

[94] G. Wei, Y. Shouwen, H. Ganyun, Finite element characterization of the size-dependent mechanical behaviour in nanosystems, Nanotechnology 17 (4) (2006) 1118–1122. doi:10.1088/0957-4484/17/4/045.

[95] M. Farsad, F. J. Vernerey, H. S. Park, An extended finite element/level set method to study surface effects on the mechanical behavior and properties of nanomaterials, International Journal for Numerical Methods in Engineering 84 (12) (2010) 1466–1489. doi:10.1002/nme.2946.

[96] S. C. Ren, J. T. Liu, S. T. Gu, Q. C. He, An XFEM-based numerical procedure for the analysis of poroelastic composites with coherent imperfect interface, Computational Materials Science 94 (2014) 173–181. doi:10.1016/j.commatsci.2014.03.047.

[97] D. P. Bach, D. Brancherie, L. Cauvin, Size effect in nanocomposites: XFEM/level set approach and interface element approach, Finite Elements in Analysis and Design 165 (2019) 41–51. doi:10.1016/j.finel.2019.07.005.

[98] H. L. Duan, X. Yi, Z. P. Huang, J. Wang, A unified scheme for prediction of effective moduli of multiphase composites with interface effects. Part I: Theoretical framework, Mechanics of Materials 39 (1) (2007) 81–93. doi:10.1016/j.mechmat.2006.02.009.

[99] A. Javili, Variational formulation of generalized interfaces for finite deformation elasticity:, Mathematics and Mechanics of Solids (Jul. 2017). doi:10.1177/1081286517719938.

[100] M. A. Crisfield, A faster modified newton-raphson iteration, Computer Methods in Applied Mechanics and Engineering 20 (3) (1979) 267–278. doi:10.1016/0045-7825(79)90002-1.

[101] M. A. Crisfield, Non-Linear Finite Element Analysis of Solids and Structures, Wiley, Chichester, 1996.

[102] H.-B. Ly, C. Desceliers, L. Minh Le, T.-T. Le, B. Thai Pham, L. Nguyen-Ngoc, V. T. Doan, M. Le, Quantification of Uncertainties on the Critical Buckling Load of Columns under Axial Compression with Uncertain Random Materials, Materials 12 (11) (2019) 1828. doi:10.3390/ma12111828.

[103] H. Saffari, M. J. Fadaee, R. Tabatabaei, Nonlinear Analysis of Space Trusses Using Modified Normal Flow Algorithm, Journal of Structural Engineering 134 (6) (2008) 998–1005. doi:10.1061/(ASCE)0733-9445(2008)134:6(998).

[104] B. Staber, J. Guilleminot, C. Soize, J. Michopoulos, A. Iliopoulos, Stochastic modeling and identification of a hyperelastic constitutive model for laminated composites, Computer Methods in Applied Mechanics and Engineering 347 (2019) 425–444. doi:10.1016/j.cma.2018.12.036.

[105] B. Staber, J. Guilleminot, A random field model for anisotropic strain energy functions and its application for uncertainty quantification in vascular mechanics, Computer Methods in Applied Mechanics and Engineering 333 (2018) 94–113. doi:10.1016/j.cma.2018.01.001.

[106] B. Staber, J. Guilleminot, Functional approximation and projection of stored energy functions in computational homogenization of hyperelastic materials: A probabilistic perspective, Computer Methods in Applied Mechanics and Engineering 313 (2017) 1–27. doi:10.1016/j.cma.2016.09.019.

[107] A. Clément, C. Soize, J. Yvonnet, Computational nonlinear stochastic homogenization using a nonconcurrent multiscale approach for hyperelastic heterogeneous microstructures analysis, International Journal for Numerical Methods in Engineering 91 (8) (2012) 799–824. doi:10.1002/nme.4293.

[108] N. S. Ottosen, M. Ristinmaa, J. Mosler, Framework for non-coherent interface models at finite displacement jumps and finite strains, Journal of the Mechanics and Physics of Solids 90 (2016) 124–141. doi:10.1016/j.jmps.2016.02.034.

[109] T. Heitbreder, N. S. Ottosen, M. Ristinmaa, J. Mosler, Consistent elastoplastic cohesive zone model at finite deformations – Variational formulation, International Journal of Solids and Structures 106-107 (2017) 284–293. doi:10.1016/j.ijsolstr.2016.10.027.

[110] T. Heitbreder, N. S. Ottosen, M. Ristinmaa, J. Mosler, On damage modeling of material interfaces: Numerical implementation and computational homogeniza-

794 tion, Computer Methods in Applied Mechanics and Engineering 337 (2018) 1–27.
795 doi:10.1016/j.cma.2018.03.023.